

## Vibrational properties of hexagonal LiBC: Infrared and Raman spectroscopy

J. Hlinka,<sup>1</sup> V. Železný,<sup>1</sup> I. Gregora,<sup>1</sup> J. Pokorný,<sup>1</sup> A. M. Fogg,<sup>2</sup> J. B. Claridge,<sup>2</sup> G. R. Darling,<sup>2</sup> and M. J. Rosseinsky<sup>2</sup>

<sup>1</sup>*Institute of Physics ASCR, Praha, Czech Republic*

<sup>2</sup>*Department of Chemistry, University of Liverpool, Liverpool L69 3BX, UK*

(Dated: February 2, 2008)

The paper presents infrared reflectivity and micro-Raman scattering spectra of LiBC powder pellets. The experiment allowed assignment of frequencies of all infrared and Raman active zone center modes:  $E_{1u}(\text{LO})$  at  $1262\text{ cm}^{-1}$  and  $381\text{ cm}^{-1}$ ,  $E_{2g}$  at  $1172\text{ cm}^{-1}$  and  $174\text{ cm}^{-1}$  and  $A_{2u}(\text{LO})$  at  $825\text{ cm}^{-1}$  and  $545\text{ cm}^{-1}$ . Results are compared with available ab-initio calculations; prediction of large Born effective charges on the nodes of B-C graphene sheets is confirmed.

LiBC is a layered boron carbide consisting of alternating graphene-like (BC)<sup>-</sup> sheets separated by intercalated Li<sup>+</sup> ions. It normally crystallizes with a hexagonal structure of  $D_{6h}^4$  (P6<sub>3</sub>/mmc) space group symmetry with Li, B and C atoms in 2a, 2c and 2d Wyckoff positions, respectively<sup>1</sup>. The structure is very close to that of the recently discovered unconventional superconductor MgB<sub>2</sub><sup>2</sup>. Electronic band structure of both materials is also quite similar, except for that LiBC is an insulator with completely filled 2p- $\sigma$  graphene bands. Since the deformation potential due to the  $E_{2g}$  zone center bond stretching mode is in LiBC even higher than in MgB<sub>2</sub><sup>3</sup>, it was predicted that the hole-doped LiBC could show superconductivity with  $T_c$  of order of 80 K. Several groups<sup>4,5,6,7,8,9</sup> tried different methods to achieve superconductivity in Li deficient samples, but none of these attempts were successful. The reason of the failure (or failure of the prediction) has not yet been elucidated. In any case, comparative LiBC *vs* MgB<sub>2</sub> studies are desirable for detailed understanding of the MgB<sub>2</sub>-type superconductivity.

Vibrational properties of LiBC were thoroughly studied by ab-initio methods<sup>9,10,11,12,13</sup>, but due to the lack of large single crystals, the desirable experimental information is quite limited.<sup>9,14,15,16</sup> Group-theoretical analysis predicts ten zone-center optic lattice modes: a pair of Raman active  $E_{2g}$  modes (B-C bond stretching mode and B-C layers sliding mode);  $2E_{1u}$  (B-C bond stretching mode and B-C layer *vs* Li layer sliding mode) and  $2A_{2u}$  (B-C layer puckering mode and B-C layer against Li layer beating mode) infrared active modes; and  $2B_{2g} + E_{2u} + B_{1u}$  optically silent modes. In this paper, we present results of a systematic room-temperature infrared and Raman spectroscopic study on polycrystalline LiBC pellets, which provides a complete spectrum of zone center optically active modes in LiBC ( $2E_{1u} + 2E_{2g} + 2A_{2u}$  species.)

Let us briefly review the previous experimental investigations of phonons in LiBC by infrared, Raman and inelastic neutron scattering spectroscopy on microcrystals and powder samples. Inelastic neutron scattering has shown weighted phonon density of states extending up to about  $1300\text{ cm}^{-1}$ , with three pronounced bands in the range  $350\text{--}450\text{ cm}^{-1}$ ,  $700\text{--}850\text{ cm}^{-1}$  and  $1000\text{--}1250\text{ cm}^{-1}$ , corresponding to external, puckering and stretching modes of the graphene-like sheets, re-

spectively (the lowest frequency band comprises also Li-ion vibrations.) A pair of Raman active  $E_{2g}$  modes was observed<sup>4,9,14</sup> near  $170\text{ cm}^{-1}$  and  $1170\text{ cm}^{-1}$ . These modes correspond to sliding of the graphene sheets and to the B-C bond stretching modes, respectively. In addition, another pair of sharp and strong Raman lines, presumably corresponding to  $B_{1g}$  modes, was seen in a metastable trigonal form of LiBC<sup>14</sup>. Two of four infrared active modes ( $E_{1u}$  species) should contribute to the reflectivity of hexagonal faces. However, the infrared microscope experiment<sup>15</sup> on a micro-crystallite with a well-developed natural hexagonal face showed a more complicated spectrum, so that only the higher frequency  $E_{1u}$  (at  $1180\text{ cm}^{-1}$ ) could be reliably assigned.<sup>15</sup> The other two infrared active modes, polarized along the hexagonal axis ( $A_{2u}$  species), should contribute together with  $E_{1u}$  modes to the infrared response of powder samples. Unfortunately, the previously published<sup>16</sup> reflectivity and transmission spectra on LiBC powder are far from the expected 4-mode spectral profile.

Samples used in this study were prepared at the University of Liverpool. Stoichiometric LiBC was synthesized in Ta ampoules at  $1773\text{ K}$  under Ar atmosphere by the method described in Refs. 1,4. The golden polycrystalline powder, handled under inert atmosphere, was characterized by laboratory x-ray diffraction test proving a single LiBC phase with lattice parameters  $a = 2.75\text{ \AA}$  and  $c = 7.05\text{ \AA}$ . On a closer inspection, small systematic shoulders on the Bragg reflections were found, indicating<sup>5</sup> a small amount of Li deficient phase with composition of about  $\text{Li}_{0.95}\text{BC}$  ( $a = 2.74\text{ \AA}$ ,  $c = 7.07\text{ \AA}$ ). The powder was then isostatically pressed to form  $0.65\text{ mm}$  thick pellets with  $8\text{ mm}$  diameter. Spectroscopic experiments were carried out in IOP ASCR in Praha within 20 hours after opening of the sealed glass ampoules containing the pellets.

The Raman experiments were carried out using a Renishaw Raman microscope with  $514.5\text{ nm}$  ( $2.41\text{ eV}$ ) argon laser excitation. The instrument allows both the direct microscope observation and measurement of polarized Raman spectra in back scattering configuration from a spot size down to 1-2 microns in diameter. To minimize heating of the sample in the laser focus, the laser power was kept below  $1\text{ mW}$ .

Surface of virgin pellets showed a dark golden-brown

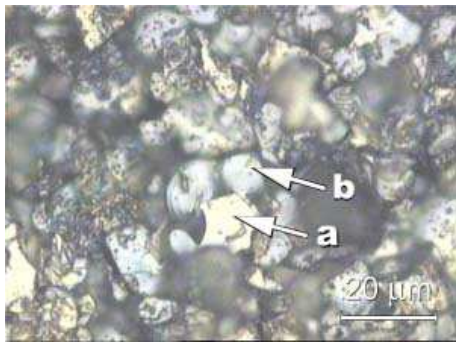


FIG. 1: (Color online) Optical microscope view of the surface of the virgin LiBC pellet, showing "yellowish" (a) and "bluish" (b) regions.

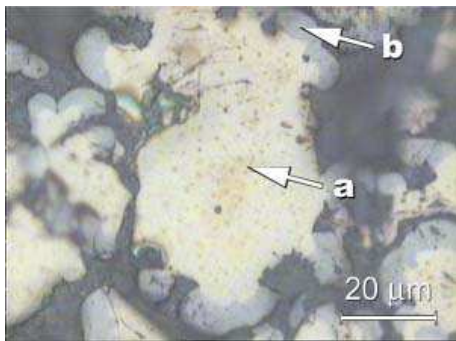


FIG. 2: (Color online) Optical microscope view of a larger grain on the surface of the partially polished LiBC pellet.

The "yellowish" (a) and "bluish" (b) regions correspond to stoichiometric (LiBC) and non-stoichiometric ( $\text{Li}_{0.95}\text{BC}$ ) compositions, respectively.

metallic appearance at naked eye view, but optical microscope observations revealed crystallites with bluish and yellowish faces with typical size of order of 10 microns. The borders of bluish faces were often rounded or kidney-shaped, while the borders of the yellowish faces were more straight (Fig. 1). Residual area corresponded to holes or black material without any Raman signal. After polishing of the surface, it became apparent that the border area of larger crystallites tends to be bluish, while the interior part is yellowish, with a well defined boundary between the bluish and yellowish regions (Fig. 2). Raman spectra of the bluish regions show a pair of  $E_{2g}$  modes near  $160\text{ cm}^{-1}$  and  $1184\text{ cm}^{-1}$  and weak, broad features  $d_1$ ,  $d_2$  and  $d_3$  reminiscent of the phonon density of states bands, superposed on a strong luminescent background (see Fig. 3). Very similar Raman spectra were observed previously on the annealed LiBC in Ref. 14. In contrast, the luminescent background was practically absent in the yellowish crystallites, and the  $E_{2g}$  lines were significantly sharper and at a somewhat "repelled" positions  $174\text{ cm}^{-1}$  and  $1172\text{ cm}^{-1}$  (see Fig. 3). Furthermore, the yellowish crystallites revealed strong asymmetric bands near  $1700\text{ cm}^{-1}$  and  $2500\text{ cm}^{-1}$ , which strongly reminis-

cent of two-phonon double resonant Raman scattering lines in graphite.<sup>17</sup> These bands, first reported in Ref. 4, indeed correspond well to doubled frequency of the puckering and B-C bond stretching vibrations, and will be investigated in more detail elsewhere. From the above observations, we conclude that the yellowish regions correspond to the stoichiometric LiBC, while bluish regions correspond to the non-stoichiometric  $\text{Li}_{0.95}\text{BC}$  component seen by X-ray diffraction.

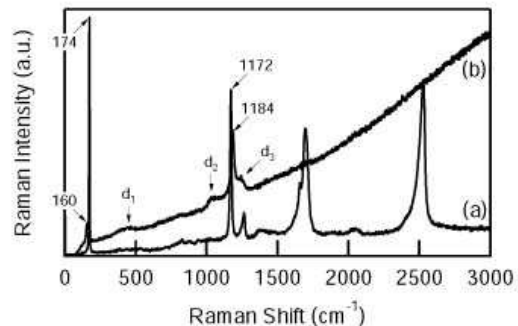


FIG. 3: Typical unpolarized Raman spectrum taken from yellowish (a) and bluish (b) part of the LiBC pellet.

Finally, let us stress that none of the Raman spectra taken from this sample showed the additional pair<sup>14</sup> of sharp and strong  $B_{1g}$ -like Raman lines near  $546\text{ cm}^{-1}$  and  $830\text{ cm}^{-1}$ , so that the present sample is clearly free from the low symmetry modification. We have observed, however, in some of the yellowish regions, a very weak but quite sharp lines near  $388\text{ cm}^{-1}$ ,  $548\text{ cm}^{-1}$  and  $828\text{ cm}^{-1}$ , which, as will be shown below, correspond surprisingly well to the LO frequencies of infrared active optic modes. We speculate that these weak features may be coupled LO phonon-plasmon modes.<sup>18</sup> In this case, such modes should be absent in cross-polarized geometry, which was indeed observed (see Fig. 4).

Infrared reflectivity at near-normal incidence was measured using a Bruker 113v spectrometer. To improve the surface quality, we tried both dry and wet polishing using diamond paste and different organic liquids, but we were not able to achieve a mirror-like reflection over the entire surface of the pellet. Therefore, we have rather measured directly the reflectivity of the as received ("virgin") surface. The absolute value of reflectivity is calculated as a ratio of the sample and Al mirror spectra. After the measurement, about 300 nm of Au was evaporated on the measured pellet surface, in order to perform an auxiliary reflectivity measurement allowing to estimate the area of highly reflecting microcrystalline faces arranged parallel to the surface. Reflectivity of these surfaces was then determined as a ratio of virgin pellet and Au-coated reflectivities.

Resulting reflectivity spectrum (Fig. 5.) shows two

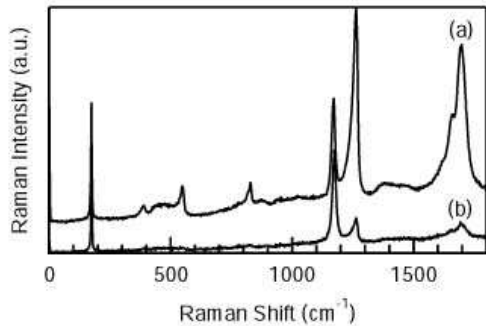


FIG. 4: Raman spectra of a yellowish crystallite showing three weak, normally forbidden lines close to LO frequencies of infrared active modes. Spectra are taken in (a) parallel and (b) perpendicular polarization conditions.

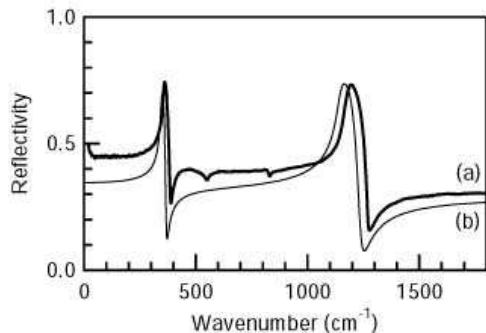


FIG. 5: Unpolarized infrared reflectivity spectrum of the LiBC. (a) Typical unpolarized experimental spectrum of the investigated LiBC pellet. (b) Theoretical single-crystal c-face reflectivity calculated from the model using *ab-initio* calculated phonon parameters (details in the text).

clear bands corresponding to  $E_{1u}$  phonon modes (with LO frequencies near  $1262 \text{ cm}^{-1}$  and  $381 \text{ cm}^{-1}$ ). This is obvious from comparison with the single-crystal reflectivity calculated for normal incidence c-face reflection

$$R_a(\omega) = \left| \frac{\sqrt{\epsilon_a(\omega)} - 1}{\sqrt{\epsilon_a(\omega)} + 1} \right|^2, \quad (1)$$

using the usual damped harmonic oscillator expression for in-plane dielectric permittivity  $\epsilon_a(\omega)$

$$\frac{\epsilon_a(\omega)}{\epsilon_a^\infty} = 1 + \frac{\Omega_1^2}{\omega_1^2 - \omega^2 - i\omega\Gamma_1} + \frac{\Omega_2^2}{\omega_2^2 - \omega^2 - i\omega\Gamma_2}, \quad (2)$$

with *ab-initio* calculated<sup>12</sup> parameters (electronic permittivity  $\epsilon_a^\infty = 11.24$ ,  $E_{1u}$ (TO) frequencies  $\omega_1 = 346 \text{ cm}^{-1}$ ,  $\omega_2 = 1143 \text{ cm}^{-1}$ , screened plasma mode frequencies  $\Omega_1 = 135 \text{ cm}^{-1}$ ,  $\Omega_2 = 469 \text{ cm}^{-1}$ ) and assuming

a reasonable damping  $\Gamma_i = 0.03\omega_i$  as in Ref. 12. The general agreement indicates that the majority of micro-crystalline faces on the surface are parallel to the hexagonal plane, as could be guessed from the typical plate-like habitus of LiBC powder grains. Two small additional dips near  $545 \text{ cm}^{-1}$  and  $825 \text{ cm}^{-1}$  are close to *ab-initio* frequencies of  $A_{2u}$ (LO) modes, suggesting that few crystallites on the surface have nevertheless a different orientation. While the values of TO and LO frequencies of  $E_{1u}$  modes could be easily adjusted to match the experimental data, the overall increase of the measured reflectance between  $1500$  and  $200 \text{ cm}^{-1}$  cannot be attributed to the dielectric contribution of these phonon modes only. This additional contribution could be an effect related to the powder form of the LiBC sample or due to a metallic impurity component in the sample etc. On the other hand, the sharp increase of the reflectivity below  $50 \text{ cm}^{-1}$  could be modeled by a Drude model with  $\omega_p^2/\Gamma_p \approx 10-20 \text{ cm}^{-1}$  what might be considered as intrinsic LiBC effect compatible with dc conductivity of LiBC<sup>7</sup>.

mode	<i>ab-initio</i>			Raman	IR
	Ref. 9	Ref. 11	Ref. 12		
$E_{2g}$	176	171	169	174	
$E_{2u}$	301	306	292		
$B_{1g}$	319	289	299		
$E_{1u}$ (TO1)	354	352	346		356
$E_{1u}$ (LO1)	382		367	(388)	381
$A_{2u}$ (TO3)	457	422	407		
$A_{2u}$ (LO3)	563		499	(548)	545
$B_{2u}$	548	540	510		
$A_{2u}$ (TO4)	819	802	803		
$A_{2u}$ (LO4)	840		833	(828)	825
$B_{1g}$	843	821	829		
$E_{1u}$ (TO2)	1136	1194	1143		1174
$E_{1u}$ (LO2)	1231		1236		1262
$E_{2g}$	1145	1204	1153	1172	

TABLE I: Frequencies of zone center modes in LiBC (in  $\text{cm}^{-1}$ ). Values in brackets correspond to the weak sharp lines discussed in the text.

Frequencies of all measured phonon modes are compared with available *ab-initio* calculations in Tab. I. From Raman measurement, only the data from the inner yellowish regions are shown. It is remarkable that the LO frequencies calculated as zeros of the adjusted dielectric permittivity coincides within  $10 \text{ cm}^{-1}$  with the LO frequencies determined from Raman measurements. Generally, the experimental frequencies of  $E_{1u}$  and of  $E_{2g}$  modes tend to be somewhat higher than the theoretical ones.

The  $E_{1u}$  mode experimental screened plasma frequencies ( $\Omega_1=147 \text{ cm}^{-1}$  and  $\Omega_2=459 \text{ cm}^{-1}$ ) are quite close to the *ab-initio* calculated values  $135$  and  $469 \text{ cm}^{-1}$ . These values can be used for evaluation of in-plane diagonal components of Born effective charge tensors. Let us

consider  $E_{1u}$  modes polarized along the x-axis. The eigenvector of the  $j$ -th mode can be defined by three nonzero components of its mass-reduced polarization vectors  $(x_{\text{Li}}(j), x_{\text{B}}(j), x_{\text{C}}(j))$ ,  $x_{\text{Li}}(j)^2 + x_{\text{B}}(j)^2 + x_{\text{C}}(j)^2 = 1$ . The screened plasma frequency of the mode ( $j$ ) is then given by

$$\Omega_j = \left| \sum_{\kappa=\text{Li,B,C}} x_{\kappa}(j) \Omega_{\text{ion},\kappa} \frac{Z_{\kappa,a}^*}{|Z_{\kappa,a}^*|} \right|, \quad (3)$$

where

$$\Omega_{\text{ion},\kappa} = \beta \frac{Z_{\kappa,a}^*}{\sqrt{m_{\kappa}}}, \quad (4)$$

is the ionic (in-plane) screened plasma frequency,  $Z_{\kappa,a}^*$  is the in-plane diagonal components of Born effective charge tensor of ion  $\kappa$  and  $m_{\kappa}$  is its relative mass. The common factor

$$\beta = \frac{e}{\sqrt{m_{\text{u}} \epsilon_0 \epsilon_{\text{a}}^{\infty} V_0}} \quad (5)$$

includes elementary charge  $e$ , atomic mass unit  $m_{\text{u}}$ , permittivity of vacuum  $\epsilon_0$ , volume of primitive unit cell  $V_0$  and relative in-plane electronic permittivity  $\epsilon_{\text{a}}^{\infty}$ .

Assuming that the lower frequency  $E_{1u}$ (TO1) mode involves purely rigid motion of graphene sheets, eigenvectors  $x_{\kappa}(j)$  of TA, TO1 and TO2  $E_{1u}$  modes are given by columns of the matrix  $T_{\kappa j} = x_{\kappa}(j)$

$$T = \begin{pmatrix} \sqrt{m_{\text{Li}}} & -\sqrt{m_{\text{BC}}} & 0 \\ \sqrt{m_{\text{B}}} & \sqrt{\frac{m_{\text{Li}} m_{\text{B}}}{m_{\text{BC}}}} & -\sqrt{\frac{m_{\text{C}} M}{m_{\text{BC}}}} \\ \sqrt{m_{\text{C}}} & \sqrt{\frac{m_{\text{Li}} m_{\text{B}}}{m_{\text{BC}}}} & \sqrt{\frac{m_{\text{B}} M}{m_{\text{BC}}}} \end{pmatrix} \frac{1}{\sqrt{M}}, \quad (6)$$

where  $m_{\text{BC}} = m_{\text{C}} + m_{\text{B}}$  and  $M = m_{\text{BC}} + m_{\text{Li}}$ . Using the experimental values of screened plasma frequencies of TO1 and TO2 modes ( $\Omega_1$  and  $\Omega_2$ ) and for  $Z_{\text{Li,a}}^* > 0$ ,  $Z_{\text{C,a}}^* < 0$ ,  $Z_{\text{Li,a}}^* + Z_{\text{B,a}}^* + Z_{\text{C,a}}^* = 0$ , eqns. (3 and (6)) yield unique solution  $\Omega_{\text{ion,Li}} = 129 \text{ cm}^{-1}$ ,  $\Omega_{\text{ion,B}} = 284 \text{ cm}^{-1}$ ,  $\Omega_{\text{ion,C}} = -367 \text{ cm}^{-1}$ . The corresponding in-plane diagonal components of Born effective charge tensors directly follows from eqs.(4) and (5), giving (for  $V_0 = 23 \text{ \AA}^3$  and  $\epsilon_{\text{a}}^{\infty} = 11.24$ )

$$Z_{\text{Li,a}}^* = 0.78, \quad Z_{\text{B,a}}^* = 2.15, \quad Z_{\text{C,a}}^* = -2.93. \quad (7)$$

These values are indeed close to *ab-initio* values<sup>12</sup> 0.81, 2.37 and -3.17.

In conclusion, although the present experiment cannot substitute single crystal measurements, we were able to observe all optically active modes of LiBC and estimate their frequencies. The screened plasma frequencies frequencies of  $E_{1u}$  modes were used to determine in-plane diagonal components of Born effective charge tensors at Li, B and C ions. The obtained results are in a perfect agreement with first-principle predictions for vibrational properties of stoichiometric LiBC.

#### Acknowledgments

The work has been supported by Czech grant project AVOZ 1-010-914.

- <sup>1</sup> M. Wörle, R. Nesper, G. Mair, M. Schwartz, and H.G. von Schnering, *Z. Anorg. Allg. Chem.* **621** 1153,(1995).
- <sup>2</sup> J. Nagamatsu, N. Nakagawa, T. Muranaka, Y. Zenitani and J. Akimitsu, *Nature* **410**, 63 (2001).
- <sup>3</sup> H. Rosner, A. Kitaigorodsky, and W. E. Pickett, *Phys.Rev.Lett.* **88**, 127001 (2002).
- <sup>4</sup> A. M. Fogg, P. R. Chalker, J. B. Claridge, G. R. Darling, and M. J. Rosseinsky, *Phys.Rev. B* **67**, 245106 (2003).
- <sup>5</sup> A. M. Fogg, J. B. Claridge, G. R. Darling, and M. J. Rosseinsky, *Chem. Commun.* 1348 (2003).
- <sup>6</sup> L. Zhao, P. Klavins, and Kai Liu, *J. Appl. Phys.* **93**, 8653 (2003).
- <sup>7</sup> D. Souptel, Z. Hossain, G. Behr, W. Lösser, Ch. Geibel, *Sol. St. Comm.* **125**, 17 (2003).
- <sup>8</sup> R. J. Cava, H. W. Zandbergen, and K. Inumaru, *Physica C* **385**, 8 (2003).
- <sup>9</sup> B. Renker, H. Schober, P. Adelman, P. Schweiss, K. B. Bohnen, and R. Heid, D. Ernst, M. Koza, P. Adelman, *cond-mat/0302036*.

- <sup>10</sup> J. M. An, S. Y. Savrasov, H. Rosner, and W. E. Pickett, *Phys.Rev. B* **66**, 220502 (2002).
- <sup>11</sup> J. M. An, H. Rosner, S. Y. Savrasov, and W. E. Pickett, *Physica B* **328** 1 (2003).
- <sup>12</sup> Kwan-Woo and W. E. Pickett, *cond-mat/0302488*.
- <sup>13</sup> J. K. Dewhurst, S. Sharma, C. Ambrosch-Draxl, and B. Jonamsson, *cond-mat/0210704*.
- <sup>14</sup> J. Hlinka, I. Gregora, J. Pokorný, A.V. Pronin, and A. Loidl, *Phys. Rev. B* **67**, 020504 (2003).
- <sup>15</sup> A.V. Pronin, K. Pucher, P. Lunkenheimer, A. Krimmel, and A. Loidl, *Phys. Rev. B* **67**, 132502 (2003).
- <sup>16</sup> A. Bharathi, S. Jemima Balaselvi, M. Premila, T.N. Sairam, G.L.N. Reddy, C.S. Sundar, and Y. Hariharan, *Sol.St. Comm.* **124**, 423 (2002).
- <sup>17</sup> C. Thomsen and S. Reich, *Phys. Rev. Lett.* **85**, 5214 (2000).
- <sup>18</sup> A. Mooradian and A. L. McWhorter, *Phys. Rev. Lett.* **19**, 849 (1967).